Characterization of Silica-Supported Pd−Au Clusters by X-ray Absorption Spectroscopy

Scott N. Reifsnyder and H. Henry Lamb*

Department of Chemical Engineering, North Carolina State University, Box 7905, Raleigh, North Carolina 27695

Received: July 7, 1998; In Final Form: November 20, 1998

Silica-supported Pd−Au clusters were characterized by Pd K and Au L_3 extended X-ray absorption fine structure (EXAFS) spectroscopy and Au $L_{2,3}$ X-ray absorption near-edge structure (XANES) spectroscopy. Pd−Au/SiO_2 catalysts with Pd/Au atomic ratios of approximately 1:1 were prepared by coadsorption of $[Pd(NH_3)_4][NO_3]_2$ and $[Au(en)_2]Cl_3$ (en = ethylenediamine) onto silica gel from pH 7 and pH 10 slurries. EXAFS spectroscopy of the Pd−Au/SiO_2 (1.3:1, pH 7) catalyst after in situ reduction at 300 °C indicates the formation of bimetallic clusters exhibiting Pd surface enrichment. The EXAFS results can be approximated using a cluster "decoration" model in which a Au-rich core is covered by a partial monolayer of Pd. In contrast, EXAFS spectroscopy of the Pd−Au/SiO_2 (1:1, pH 10) catalyst after in situ reduction at 350 °C indicates the formation of homogeneous Pd−Au alloy clusters. The homonuclear bond distances in these clusters agree closely with the Vegard's Law prediction for a 1:1 Pd−Au alloy; however, the heteronuclear bond distances are ∼0.02 Å shorter. Au $L_{2,3}$ XANES spectroscopy of the supported Pd−Au clusters evidences a vanishingly small density of unoccupied Au 5d states. Excellent correspondence is observed between the XANES spectra of supported Pd−Au clusters and those of Pd−Au alloy films having similar compositions.

Introduction

Supported bimetallic catalysts are used in a variety of applications, including naphtha reforming, automobile pollution control, and chemical manufacturing. Supported Pd−Au catalysts are employed commercially for vinyl acetate (VA) synthesis from ethylene, acetic acid, and oxygen. The addition of catalytically inactive Au to supported Pd results in a catalyst exhibiting higher VA selectivity and better activity maintenance.[1,2] The performance (e.g., activity, selectivity, activity maintenance) of a monometallic catalyst can be altered by addition of a less active (or inactive) metal via two basic mechanisms: charge transfer (ligand effects) and structural modification of surface sites (ensemble effects).[3] In principle, charge transfer between surface Pd and Au atoms can alter the strength of Pd−adsorbate bonds; however, recent experiments have provided no conclusive evidence of ligand effects in supported Pd−Au catalysts.[4] Dilution of surface Pd atoms by inert Au atoms can modify multiatom sites (ensembles) required for structure-sensitive reactions.[5] Consequently, knowledge of the surface composition of bimetallic clusters is critical to understanding the properties of supported bimetallic catalysts.

Extended X-ray absorption fine structure (EXAFS) spectroscopy is a particularly valuable technique for elucidating the structures of supported bimetallic catalysts.[6] By analyzing the EXAFS spectrum of each metal, one obtains two independent, yet necessarily consistent, sets of structural parameters.[7] Lam and Boudart[8] prepared Pd−Au/SiO_2 catalysts from $[Pd(NH_3)_4][NO_3]_2$ and $[Au(en)_2]Cl_3$ (en = ethylenediamine) and characterized them by Mössbauer spectroscopy, chemisorption, and X-ray line broadening. They concluded that the supported bimetallic catalysts contained homogeneous Pd−Au alloy clusters. In contrast, a recent EXAFS spectroscopy study[9] of similarly prepared catalysts indicated that the supported clusters had a Au-rich core decorated by Pd atoms. These results, however, were only semiquantitative as the Pd and Au edge EXAFS results did not satisfy the consistency criterion proposed by Via et al.[7] Clearly, the EXAFS analysis of these catalysts can be improved. Moreover, a better understanding of the influence of catalyst preparation conditions on the structure and properties of supported Pd−Au clusters is warranted.

In this work, we investigated the structures of silica-supported Pd−Au clusters prepared using variations on the method of Lam and Boudart.[8] The reduced catalysts were characterized by Pd K and Au $L_{2,3}$ edge X-ray absorption spectroscopy (XAS). The Au $L_{2,3}$ X-ray absorption near-edge structure (XANES) spectra of silica-supported Au clusters and a series of Pd−Au alloy films were also measured and used in interpreting the data for the supported Pd−Au clusters.

Experimental Methods

Catalyst Preparation. *Au/SiO_2.* A 1 wt % Au/SiO_2 catalyst was prepared by incipient wetting with an aqueous solution of $[Au(en)_2]Cl_3$ (en = ethylenediamine). Incipient wetness impregnation was employed because we observed negligible adsorption of $[Au(en)_2]Cl_3$ on silica gel from aqueous solution at 25 °C. A thick paste was formed from SiO_2 (Degussa, 300 m^2/g, 3.0 g) and a solution of $[Au(en)_2]Cl_3$ (15 mg) in deionized (DI) water (8.0 mL). The paste was dried in air at 100 °C yielding a mauve powder. The Au/SiO_2 catalyst was subsequently reduced in flowing H_2 at 300 °C for 1 h. The catalyst was cooled in H_2 to <50 °C and purged with He before exposure to air at 30 °C.

Pd−Au/SiO_2. SiO_2 (Degussa, 300 m^2/g) was washed with DI water and dried in air at 100 °C. An aqueous solution containing $[Pd(NH_3)_4][NO_3]_2$ and $[Au(en)_2]Cl_3$ was added dropwise to a pH 7 slurry of SiO_2 (4 g) and DI water (80 mL) at 25 °C. After a contact time of 24 h, the solid was recovered by filtration,

* To whom correspondence should be addressed. Phone: (919) 515-6395. Fax: (919) 515-3465. E-mail: lamb@eos.ncsu.edu.

10.1021/jp982893b CCC: $18.00
Published on Web 12/29/1998

washed with DI water, and dried in air at 100 °C. The resulting purplish-brown powder was dried in flowing He at 200 °C for 1 h and then reduced in flowing H_2 at 150 °C for 1 h. The reduced catalyst was cooled in flowing H_2 to <50 °C and purged with He before air exposure at 30 °C. The resulting catalyst, Pd−Au/SiO_2 (1.3:1, pH 7), contained 0.4 wt % Pd and 0.6 wt % Au for a Pd/Au atomic ratio of 1.3:1. A second Pd−Au/SiO_2 catalyst was prepared using a similar procedure except the pH of the initial SiO_2−water slurry was adjusted to 10 by NH_4OH addition. The resulting catalyst, Pd−Au/SiO_2 (1:1, pH 10), contained 0.5 wt % Pd and 0.9 wt % Au for a Pd/Au atomic ratio of 1:1. Selected samples were analyzed for Pd and Au by Galbraith Laboratories; metal loadings for the remaining samples were estimated from the Pd K and Au L_3 X-ray absorption edge step heights.

XAS. X-ray absorption measurements were made on beamline X-11A of the National Synchrotron Light Source at Brookhaven National Laboratory. The storage-ring energy was 2.5 GeV, and the current decayed from 250 to 110 mA during a typical fill. The beamline monochromator was equipped with a pair of Si(111) crystals. For Au edge XAS, the I_0 ionization chamber contained flowing 20% Ar/N_2 and the I chamber contained flowing Ar. For Pd edge XAS, the I_0 chamber contained flowing Ar and the I chamber contained static Kr.

The in situ XAS cells and catalyst treatment station have been described previously.[10] The passivated Au/SiO_2 catalyst was reduced in flowing H_2 at 100 °C, and the XA spectrum was measured under static H_2 at approximately −173 °C. The passivated Pd−Au/SiO_2 catalysts were dried in vacuo at 200 °C for 0.5 h and cooled to <30 °C. The catalysts were then reduced at either 300 °C [Pd−Au/SiO_2 (1.3:1, pH 7)] or 350 °C [Pd−Au/SiO_2 (1:1, pH 10)] for 1 h in flowing H_2, and the XA spectra were measured under static H_2 after cooling to approximately −173 °C. Subsequently, each catalyst was heated under vacuum at 150 °C [Pd−Au/SiO_2 (1.3:1, pH 7)] or 300 °C [Pd−Au/SiO_2 (1:1, pH 10)] for 1 h. After being cooled to 30 °C in vacuo, the cell was backfilled with He, and the XA spectra were measured at approximately −173 °C.

Normalized EXAFS spectra were isolated from the experimental data using standard procedures,[11] and the resulting χ function was Fourier transformed and fit in r space.[12] The Pd−Pd and Au−Au references were derived from the EXAFS spectra of Pd and Au foils, respectively, measured at −196 °C. The Pd−Au and Au−Pd references were calculated using the FEFF3 package ($N = 12$, $R = 2.80$ Å, $\sigma^2 = 0.0020$ Å^2).[13]

The XANES spectra were isolated using a variation of the procedure described by Mansour et al.[14] The contribution due to background electrons was removed by fitting the pre-edge region (−200 to −20 eV relative to the edge) to the Victoreen expression and subtracting the extrapolated values from the entire spectrum. The slowly oscillating background in the EXAFS region was fit with a cubic spline function, and the spectrum was normalized using the step height determined at 50 eV. The normalized XANES spectra of a 25 μm Au foil measured at −196 °C were used as references. The Au L_2 (L_3) reference spectrum was aligned at the Au edge (−20 < eV < 2) with the catalyst spectrum, and the reference spectrum was subtracted from the catalyst spectrum. The energy scale in the XANES difference spectra is relative to the edge inflection point.

A series of 1000 Å Pd−Au alloy films was prepared by sputter deposition from bulk alloy targets (Johnson-Mathey) onto glass slides. X-ray diffraction measurements were made to confirm the alloy compositions. The metal−metal bond distances determined by X-ray diffraction for the 60% and 80% Au alloys were in good agreement with Vegard's Law. Au $L_{2,3}$ XAS measurements were made at room temperature using fluorescence detection with an Ar-filled ionization chamber. The incident X-ray beam struck the sample at a 45° angle. The fluorescence signal (I_F) was ratioed to the incident beam intensity (I_0), and the XANES spectra were isolated using the background subtraction and normalization procedures described above.

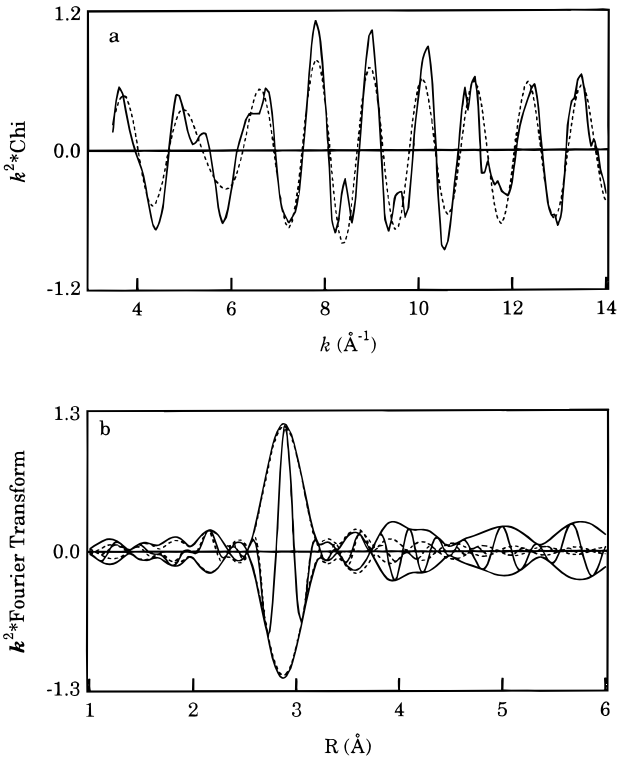

Figure 1. Au L_3 EXAFS data (solid line) and calculated first-shell fit (dashed line) in k and r space for a 1 wt % Au/SiO_2 catalyst after in situ reduction at 100 °C: (a) k^2-weighted χ function; (b) k^2-weighted Au−Au phase-corrected FT.

TABLE 1: EXAFS Fitting Parameters for 1 wt % Au/SiO_2 Catalyst

treatment	backscatterer	N^a	R^b	$\Delta\sigma^{2\,c}$	$\Delta E_0{}^d$
H_2/300 °C	Au	9.5	2.87	0.0027	0.4

[a] Coordination number (±15%). [b] NN distance (±0.01 Å). [c] Debye−Waller factor (±15%). [d] Inner potential correction (±1 eV).

Results and Data Analysis

EXAFS Spectroscopy. *Au/SiO_2 Catalyst.* The Au L_3 EXAFS spectrum of the 1 wt % Au/SiO_2 catalyst after in situ reduction in flowing H_2 at 100 °C is shown in Figure 1a. The Au−Au phase-corrected Fourier transform (FT) (Figure 1b) reveals a prominent first-shell peak and significant higher shell contributions. The first-shell contribution was fit in r space ($2.5 < r < 3.3$ Å) using a Au foil reference. The results (Table 1) indicate that the catalyst contains Au clusters that are 25−35 Å in size; a bulklike nearest neighbor (NN) distance and a low Debye−Waller factor are observed. Comparisons of the experimental and calculated EXAFS in k and r space are shown in Figure 1. The lack of agreement between the experimental and calculated χ functions in k space arises from higher shell contributions, as evidenced in Figure 1b.

Pd−Au/SiO_2 Catalysts. To ensure that physically meaningful results were obtained by analysis of the Pd K and Au L_3 edge EXAFS spectra, three consistency criteria were adopted.

(1) The heteronuclear bond distances determined from the Pd and Au EXAFS spectra should be equivalent within experimental uncertainty (±0.01 Å).

$$R_{\mathrm{Pd-Au}} = R_{\mathrm{Au-Pd}}$$

(2) The ratio of the heteronuclear coordination numbers should satisfy (within experimental uncertainty) the conservation equation:[7]

$$\frac{N_{\mathrm{Pd-Au}}}{N_{\mathrm{Au-Pd}}} = \frac{X_{\mathrm{Au}}}{X_{\mathrm{Pd}}}$$

(where, for example, $N_{\mathrm{Pd-Au}}$ is the heteronuclear coordination number at the Pd edge and X_{Pd} is the Pd atomic fraction in the sample)

(3) The Debye−Waller factors of the heteronuclear bonds should be approximately equal.

$$\Delta\sigma^2_{\mathrm{Pd-Au}} \approx \Delta\sigma^2_{\mathrm{Au-Pd}}$$

The first two criteria apply rigorously to any bimetallic system, irrespective of the state of aggregation or intermixing. The third criterion is an approximate guideline based on the assumption that the static and dynamical contributions to disorder will be similar for each absorber−backscatterer pair in a random substitutional alloy. When the Pd K and Au L_3 EXAFS spectra were fit independently, the initial results typically satisfied the first and third criteria. The initial results were adjusted manually to achieve better agreement with the second consistency criterion. Only a modest sacrifice in fit quality was required, and the results are presented below.

The Au L_3 EXAFS spectrum of a Pd−Au/SiO_2 catalyst (1.3:1, pH 7) following in situ reduction at 300 °C is shown in Figure 2a. In contrast to the spectrum in Figure 1a, interference is observed between the EXAFS signals of first-shell Pd and Au backscatterers, most notably in the region between 5 and 7 $Å^{-1}$; the effects are more apparent in the FT spectrum. The Au−Au phase-corrected FT (Figure 2b) consists of a primary peak at ∼2.7 Å and a secondary peak at ∼3.5 Å, which overlaps with the second metal−metal shell. The imaginary part of the FT is distorted and peaks negatively at ∼2.7 Å, indicating that the primary peak does not arise from a single Au−Au contribution. The *r* space fitting results ($2.0 < r < 3.8$ Å) using Au−Au and Au−Pd contributions are given in Table 2. Overall, the agreement between the experimental and calculated EXAFS spectra in *k* and *r* space is good, as shown in Figure 2. A total Au coordination number of 10.8 is found, indicating that the Au atoms occupy high-coordination environments, e.g., in the core of large bimetallic clusters. The Au−Au and Au−Pd NN distances fall between those of bulk Pd (2.75 Å) and bulk Au (2.88 Å), consistent with alloy formation; however, the Au−Au NN distance is significantly greater that the Au−Pd distance.

The Pd K EXAFS spectrum of the Pd−Au/SiO_2 (1.3:1, pH 7) catalyst following in situ reduction at 300 °C is shown in Figure 3a. The interference between 5 and 7 $Å^{-1}$, albeit weaker than that at the Au edge, is indicative of alloy formation. The Pd−Pd phase-corrected FT (Figure 3b) exhibits a first-shell peak near 2.8 Å with a large low-*r* sidelobe; higher metal−metal shells are not apparent. The *r* space fitting results ($1.8 < r < 3.4$ Å) using Pd−Pd and Pd−Au contributions are given in Table 2. Excellent fits were achieved in *k* and *r* space, as shown in Figure 3. The total Pd coordination number is only 5.9, indicating the Pd is present in small clusters or preferentially occupies surface sites in large bimetallic clusters. The Pd−Pd NN distance is greater than the Pd−Au NN distance, although both distances lie between those of the bulk metals.

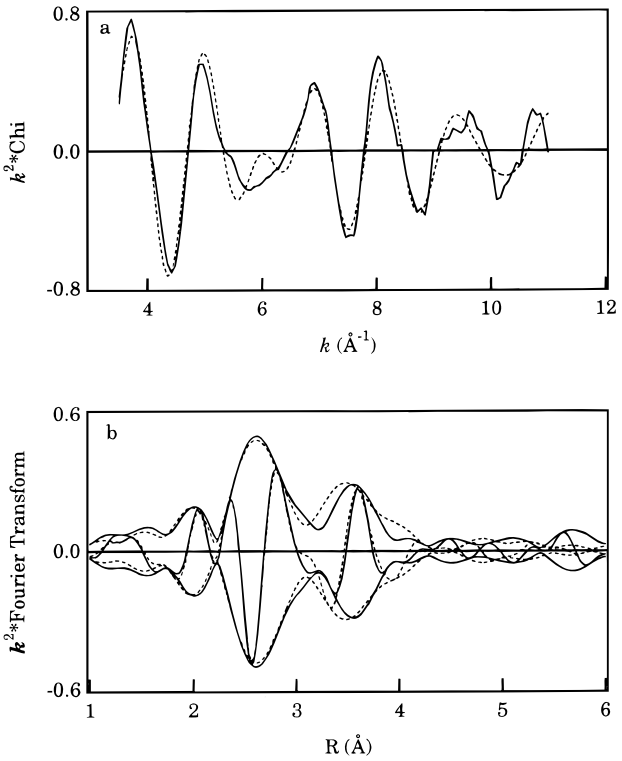

Figure 2. Au L_3 EXAFS data (solid line) and calculated first-shell fit (dashed line) in *k* and *r* space for Pd−Au/SiO_2 (1.3:1, pH 7) catalyst after in situ reduction at 300 °C: (a) k^2-weighted χ function; (b) k^2-weighted Au−Au phase-corrected FT.

The Au L_3 and Pd K EXAFS spectra of Pd−Au/SiO_2 (1.3:1, pH 7) following reduction at 300 °C and subsequent evacuation at 150 °C are similar to those of the reduced catalyst under H_2. The *r* space fitting parameters for the Au edge ($2.0 < r < 3.8$ Å) and Pd edge ($1.8 < r < 3.5$ Å) spectra are given in Table 2. The coordination numbers are equivalent (within experimental uncertainty) to those observed before evacuation; however, a decrease in the Pd−Pd NN distance and a concomitant decrease in the Debye−Waller factor are observed. The remaining bond distances are essentially unchanged; however, the Au−Pd and Pd−Au Debye−Waller factors have increased.

The Au L_3 EXAFS spectrum of the Pd−Au/SiO_2 (1:1, pH 10) catalyst following in situ reduction at 350 °C is shown in Figure 4a. The destructive interference between 5 and 7 $Å^{-1}$ that arises from the presence of first-shell Pd and Au backscatterers is more pronounced than in Figure 2a. The Au−Au phase-corrected FT (Figure 4b) is similar to Figure 2b and contains two peaks arising from the superposition of Au−Au and Au−Pd EXAFS functions. The results of an *r* space fit ($1.8 < r < 3.7$ Å) are given in Table 3. The agreement between the experimental and calculated EXAFS spectra is excellent, as shown in Figure 4. The Au−Au coordination number is significantly smaller than that of the Pd−Au/SiO_2 (1.3:1, pH 7) catalyst, although the Au−Pd coordination numbers are equivalent. The Au−Au and Au−Pd NN distances lie between those of bulk Au and bulk Pd.

The Pd K EXAFS spectrum of the Pd−Au/SiO_2 (1:1, pH 10) catalyst following in situ reduction at 350 °C is shown in Figure 5a. Interference is observed between 5 and 7 $Å^{-1}$, indicative of Pd−Au alloy formation. The Pd−Pd phase-corrected FT contains a first-shell peak with a large low-*r*

TABLE 2: Pd K and Au L_3 EXAFS Fitting Parameters for Pd−Au/SiO_2 (1.3:1, pH 7) Catalyst

treatment	absorber	back-scatterer	N^a	R^b	$\Delta\sigma^{2\,c}$	$\Delta E_0{}^d$	back-scatterer	N^a	R^b	$\Delta\sigma^{2\,c}$	$\Delta E_0{}^d$
H_2/300 °C	Pd	Pd	2.4	2.80	0.0032	3.3	Au	3.5	2.77	0.0045	2.7
	Au	Au	6.8	2.83	0.0044	2.0	Pd	4.0	2.78	0.0046	−5.3
H_2/300 °C;	Pd	Pd	2.4	2.78	0.0021	−0.6	Au	3.8	2.78	0.0065	−6.7
Vac/150 °C	Au	Au	6.6	2.83	0.0048	2.2	Pd	4.0	2.79	0.0065	−6.2

[a] Coordination number (±15%). [b] NN distance (±0.01 Å). [c] Debye−Waller factor (±15%). [d] Inner potential correction (±1 eV).

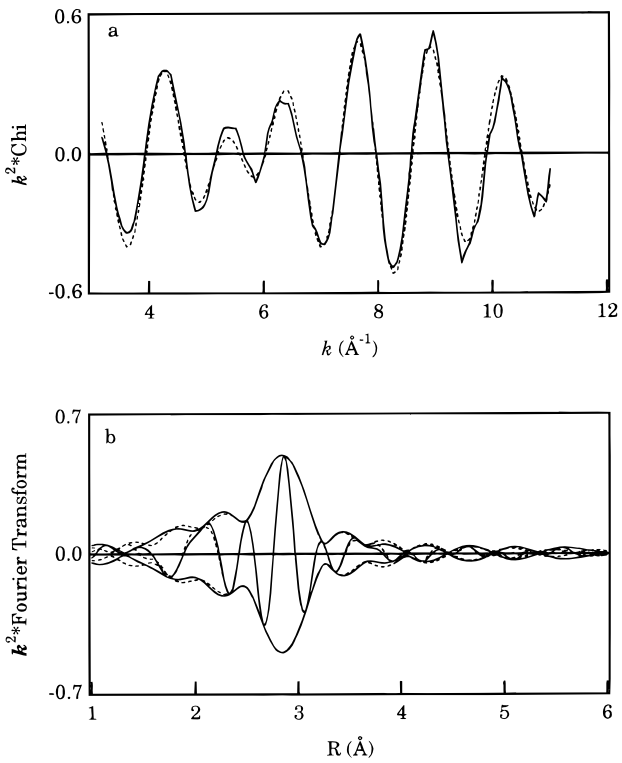

Figure 3. Pd K EXAFS data (solid line) and calculated first-shell fit (dashed line) in k and r space for Pd−Au/SiO_2 (1.3:1, pH 7) catalyst after in situ reduction at 300 °C: (a) k^2-weighted χ function; (b) k^2-weighted Pd−Pd phase-corrected FT.

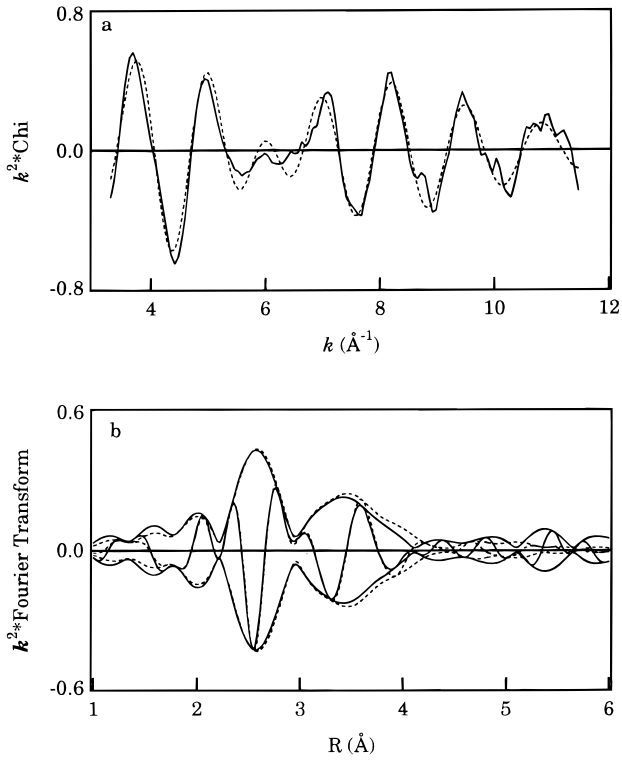

Figure 4. Au L_3 EXAFS data (solid line) and calculated first-shell fit (dashed line) in k and r space for Pd−Au/SiO_2 (1:1, pH 10) catalyst after in situ reduction at 350 °C: (a) k^2-weighted χ function; (b) k^2-weighted Au−Au phase-corrected FT.

sidelobe (Figure 5b). The results of an r space fit ($1.9 < r < 3.4$ Å) using Pd−Pd and Pd−Au contributions are given in Table 3, and the experimental and calculated EXAFS spectra are compared in k and r space in Figure 5. In contrast to the results for the Pd−Au/SiO_2 (1.3:1, pH 7) catalyst (Table 2), the observed Pd−Pd NN distance is equivalent to the Au−Au NN distance. Moreover, the total Pd and Au coordination numbers are equivalent, indicating the absence of surface enrichment in either metal.

The Au and Pd EXAFS spectra of the Pd−Au/SiO_2 (1:1, pH 10) catalyst following reduction at 350 °C and subsequent evacuation at 300 °C are closely similar to those of the reduced catalyst under H_2. The r space fitting parameters for the Au ($1.8 < r < 3.7$ Å) and Pd ($1.8 < r < 3.4$ Å) EXAFS spectra are presented in Table 3. The coordination numbers and NN distances are equivalent to those measured before evacuation; however, the Debye−Waller factors are lower.

XANES Spectroscopy. *Au/SiO_2 and Pd−Au/SiO_2 Catalysts.* The normalized Au L_3 XANES spectra of a Au foil and the Au/SiO_2 catalyst after in situ reduction at 100 °C are shown in parts a and b of Figure 6, respectively. The spectra are nearly identical. A small edge resonance (white line) is observed near 3 eV, and there are additional XANES features in the 10−50 eV range. The Au L_3 XANES spectrum of the Pd−Au/SiO_2 (1.3:1, pH 7) catalyst after impregnation and drying in air at 100 °C is shown in Figure 6d. The edge resonance is significantly more intense than that in Figure 6b; moreover, the XANES features associated with metallic Au coordination are weaker and are shifted to higher energies. The Au L_3 XANES spectrum of the Pd−Au/SiO_2 (1.3:1, pH 7) catalyst after in situ reduction at 300 °C is shown in Figure 6c. The edge resonance is weaker than that observed for metallic Au, and the XANES features at 27 and 50 eV are less intense.

The normalized Au $L_{2,3}$ XANES spectra of a Au foil and the Pd−Au/SiO_2 (1:1, pH 10) catalyst after in situ reduction at 350 °C and subsequent evacuation at 300 °C are compared in Figure 7. There is a glitch in the Au foil L_2 XANES spectrum at 11 eV. Difference spectra, which were obtained by subtracting the Au foil XANES spectra from those of the catalyst, are also shown. The L_3 difference spectrum contains a sharp negative peak at 3 eV, resulting from the lower white line intensity of the Pd−Au/SiO_2 catalyst. This peak is extremely weak (or entirely absent) in the L_2 difference spectrum; the small positive peak near the origin is ascribed to slight misalignment of the edges. Additional negative peaks are observed at 27 and 48 eV in the L_2 and L_3 XANES difference spectra. These peaks are broader in the L_2 difference spectrum, as are the corresponding features in the Au foil L_2 XANES spectrum. A broad positive peak is observed at 15 eV in the L_2 edge difference spectrum. A positive peak is also present at 15 eV in the L_3 edge difference spectrum; however, it is superimposed on the "sidelobes" of the strong negative peaks at 3 and 27 eV.

TABLE 3: Pd K and Au L_3 EXAFS Fitting Parameters for Pd−Au/SiO_2 (1.3:1, pH 7) Catalyst

treatment	absorber	back-scatterer	N^a	R^b	$\Delta\sigma^{2\,c}$	$\Delta E_0{}^d$	back-scatterer	N^a	R^b	$\Delta\sigma^{2\,c}$	$\Delta E_0{}^d$
H_2/350 °C	Pd	Pd	4.3	2.81	0.0065	2.9	Au	4.2	2.78	0.0055	−0.1
	Au	Au	4.7	2.81	0.0065	3.2	Pd	4.0	2.79	0.0061	−6.0
H_2/350 °C;	Pd	Pd	4.2	2.81	0.0052	2.4	Au	4.0	2.79	0.0047	3.3
Vac/300 °C	Au	Au	4.6	2.81	0.0038	2.6	Pd	4.0	2.78	0.0040	−7.5

[a] Coordination number (±15%). [b] NN distance (±0.01 Å). [c] Debye−Waller factor (±15%). [d] Inner potential correction (±1 eV).

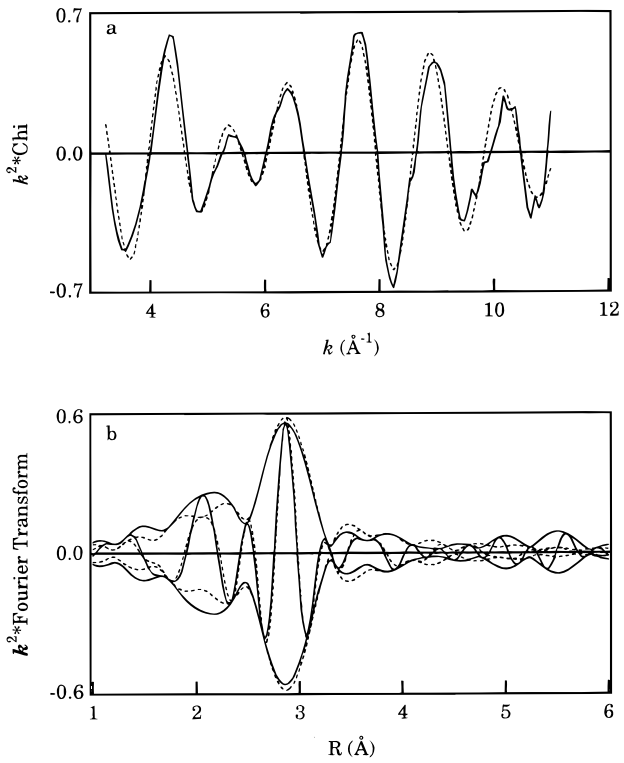

Figure 5. Pd K EXAFS data (solid line) and calculated first-shell fit (dashed line) in k and r space for Pd−Au/SiO_2 (1:1, pH 10) catalyst after in situ reduction at 350 °C: (a) k^2-weighted χ function; (b) k^2-weighted Pd−Pd phase-corrected FT.

The $L_{2,3}$ XANES difference spectra of the Pd−Au/SiO_2 (1:1, pH 10) and Pd−Au/SiO_2 (1.3:1, pH 7) catalysts following in situ reduction and evacuation are compared in Figure 8. The L_3 difference spectra are closely similar; however, the peaks are less intense, and there is significantly less positive area in the difference spectrum of the Pd−Au/SiO_2 (1.3:1, pH 7) catalyst. The L_2 difference spectra show significant deviations in the 15−50 eV region. The features are diminished in intensity, and the negative peak at 28 eV is shifted to higher energy in the difference spectrum of the Pd−Au/SiO_2 (1.3:1, pH 7) catalyst.

Pd−Au Alloy Films. The Au $L_{2,3}$ XANES difference spectra of a series of 1000 Å Pd−Au alloy films are shown in Figure 9. Although the data are somewhat noisy, the spectral features are in excellent agreement with those found in the difference spectra of the Pd−Au/SiO_2 catalysts (Figure 8). The L_3 difference spectra are dominated by two sharp negative peaks (3 and 26 eV) that are relatively insensitive to alloy composition. In contrast, the dominant feature of the L_2 difference spectra is a positive peak at 15 eV that increases in intensity with increasing Pd content. The intensities of the L_3 peak at 15 eV and the weak positive L_2 and L_3 peaks at 50−55 eV exhibit a similar trend with alloy composition. Conversely, the negative L_2 difference peak at 28 eV appears to diminish in intensity and shift to higher energy as the Pd content of the alloy decreases.

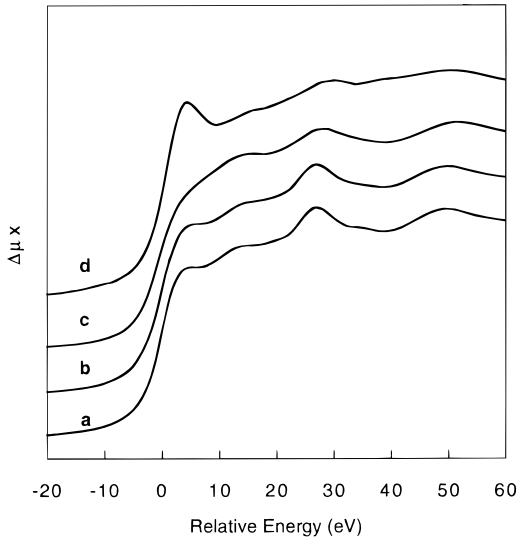

Figure 6. Comparison of the normalized Au L_3 XANES spectra of (a) Au foil, (b) 1 wt % Au/SiO_2 catalyst after in situ reduction at 100 °C, (c) Pd−Au/SiO_2 (1.3:1, pH 7) catalyst after in situ reduction at 300 °C, and (d) Pd−Au/SiO_2 (1.3:1, pH 7) catalyst after impregnation and drying in air at 100 °C.

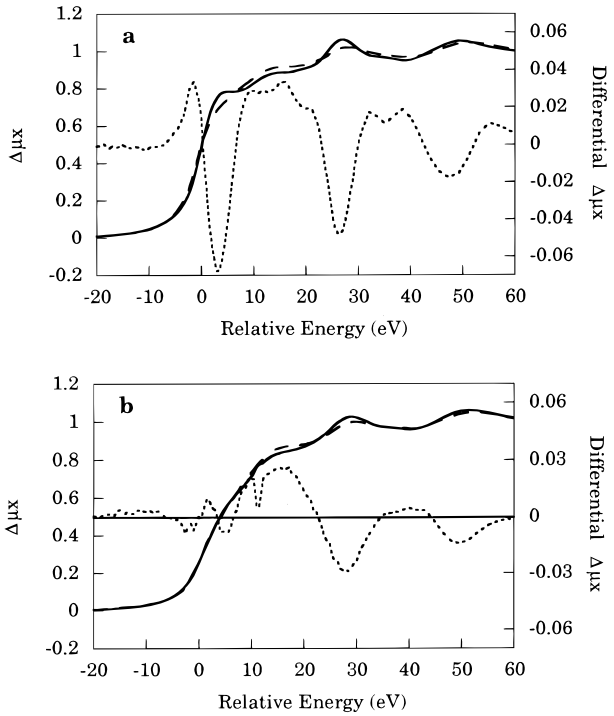

Figure 7. Normalized Au L_3 (a) and L_2 (b) XANES spectra of Pd−Au/SiO_2 (1:1, pH 10) catalyst after in situ reduction at 350 °C and subsequent evacuation at 300 °C (long dashes), a Au foil reference (solid line), and the difference spectra (short dashes).

Discussion

Pd and Au are miscible in all proportions, forming random substitutional alloys with fcc crystal structures. The lattice

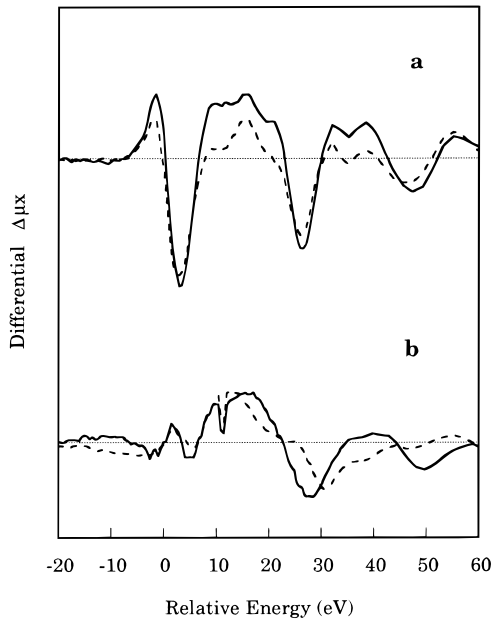

Figure 8. Normalized Au L_3 (a) and L_2 (b) XANES spectra of the Pd−Au/SiO_2 (1:1, pH 10) (solid line) and Pd−Au/SiO_2 (1.3:1, pH 7) (dashed line) catalysts following in situ reduction and subsequent evacuation.

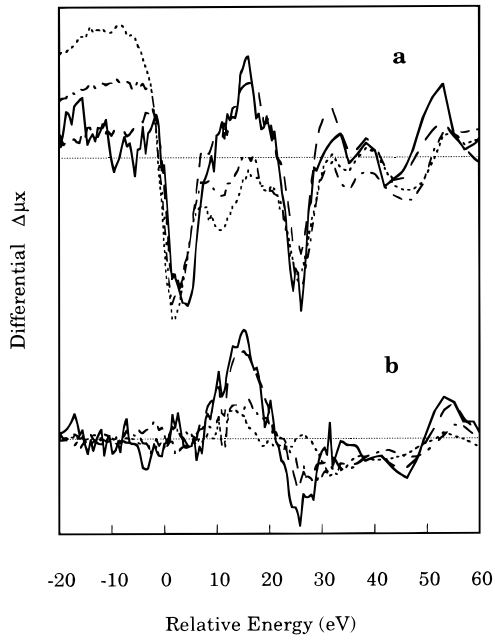

Figure 9. Normalized Au L_3 (a) and L_2 (b) XANES spectra of Pd−Au alloy films: 20% Au (solid); 40% Au (long dashes); 60% Au (dash−dot); 80% Au (short dashes)

parameters of Pd−Au alloys conform closely to Vegard's Law, increasing linearly from that of Pd (3.89 Å) to that of Au (4.08 Å) with increasing Au content. The formation of Pd−Au alloys is an exothermic process ($\Delta H_{mix} < 0$); the heat of mixing ($-\Delta H_{mix}$) reaches a maximum (~2 kcal/mol) at 60% Au.[15] The surface compositions of supported Pd−Au clusters are determined by intrinsic thermodynamic properties and kinetic variables inherent in catalyst preparation. The thermodynamic variables include ΔH_{mix}, the surface free energies of Pd and Au, the surface free energy of the support, and the heats of adsorption of any adsorbates. The kinetic variables include the reduction rate parameters for the Pd and Au precursors and the diffusion coefficients (surface and bulk) of Pd and Au atoms.

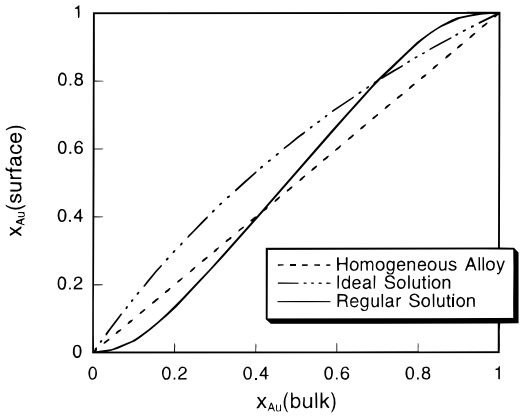

Figure 10. Surface enrichment in Pd−Au alloys. Surface composition at 27 °C as a function of bulk composition for the ideal solution and regular solution models.

The *equilibrium* surface compositions of bare, noninteracting Pd−Au crystallites can serve as a basis for comparison to actual structures. For this purpose, equilibrium surface compositions were estimated using the ideal solution and regular solution models.[3] The surface free energy difference between Pd and Au determines the surface composition in the ideal solution model ($\Delta H_{mix} = 0$).

$$\frac{x_2^s}{x_1^s} = \frac{x_2^b}{x_1^b} \exp\left\{\frac{a(\gamma_1 - \gamma_2)}{RT}\right\} \tag{1}$$

where x^s is the surface mole fraction, x^b is the bulk mole fraction, a is the molar surface area, and γ_i is the pure component surface free energy. An empirical correlation for transition metals relates γ to the heat of sublimation, ΔH_{sub}:

$$\gamma a \approx 0.16 \Delta H_{sub} \tag{2}$$

The heats of sublimation of Pd and Au are 90 and 88 kcal/mol, respectively, and the ideal solution model predicts modest Au surface enrichment over the entire composition range (Figure 10). The regular solution model accounts for deviations from ideality due to heat of mixing effects by introducing the alloy parameter Ω.

$$\Omega = N_A z\left(E_{1,2} - \frac{E_{1,1} + E_{2,2}}{2}\right) \tag{3}$$

where the $E_{i,j}$ are the $i-j$ metal−metal bond energies, N_A is Avogadro's number, and z is the bulk coordination number. Omega is related to ΔH_{mix} by

$$\Omega = \frac{\Delta H_{mix}}{x_1^b x_2^b} \tag{4}$$

The surface composition using a monolayer approximation of the regular solution model is given by

$$\frac{x_2^s}{x_1^s} = \frac{x_2^b}{x_1^b} \exp\left\{\frac{a(\gamma_1 - \gamma_2)}{RT}\right\} \exp\left\{\frac{\Omega(l+m)}{RT}[(x_1^b)^2 - (x_2^b)^2] + \frac{\Omega l}{RT}[(x_2^s)^2 - (x_1^s)^2]\right\} \tag{5}$$

where l is the fraction of nearest neighbors in the plane and m is fraction of nearest neighbors below the plane. An average Ω value of −7440 cal/mol for Pd−Au alloys was estimated from

TABLE 4: Comparison of EXAFS-Determined Coordination Numbers for Pd−Au/SiO_2 (1.3:1, pH 7) Catalyst with Cluster "Decoration" Model

			effect on model[a]	
	Pd−Au/SiO_2 (1.3:1, pH 7)	model	(1) lower Pd/Au	(2) bulk Pd
Pd/Au	1.3	2.3	↓	↔
N_{AuAu}	6.8	7.6	↔	↓
N_{AuPd}	4.0	4.4	↓	↑
N_{PdPd}	2.4	5.9	↓	↓
N_{PdAu}	3.5	1.9	↔	↑

[a] Expected model results if (1) the actual Pd/Au is less than that required for a monolayer of Pd and (2) if Pd diffuses into the Au bulk. Effect is to (↑) increase, (↓) decrease, or (↔) not change the model value.

Darby's heat of mixing data.[15] As illustrated in Figure 10, the regular solution model predicts equal surface and bulk compositions for 40% Au alloys, Pd surface enrichment for alloys containing <40% Au, and Au surface enrichment for alloys containing >40% Au. The extent of surface enrichment, however, is small over most of the composition range. Thus, extrinsic factors, such as the presence of adsorbates, are expected to significantly affect surface enrichment in Pd−Au alloys. The available experimental data support this hypothesis. Auger electron spectroscopy (AES) studies of bulk Pd−Au alloys evidence little surface enrichment after treatments in inert environments.[16,17] In contrast, annealing in H_2, H_2S, and O_2 has been shown to favor Pd surface enrichment.[16,18]

The EXAFS results for the Pd−Au/SiO_2 (1.3:1, pH 7) catalyst are consistent with Pd−Au clusters in which Pd is enriched at the surface, in agreement with the previous EXAFS study of silica-supported Pd−Au clusters by Davis et al.[9] The total Au coordination number is higher than the total Pd coordination number by almost a factor of 2, indicating that the Au preferentially occupies bulk sites. Although the overall composition of the catalyst is slightly Pd-rich, the first coordination shells of Pd and Au each contain approximately 60% Au, and the Au−Au NN distance agrees closely with the Vegard's Law prediction for an 60% Au alloy. The close similarity of the Au $L_{2,3}$ XANES difference spectra of the Pd−Au/SiO_2 (1.3:1, pH 7) catalyst (Figure 8) and those of the Pd−Au alloy films (Figure 9) indicates that most of the Au in the catalyst is alloyed with Pd. Evacuation at 150 °C leads to a small contraction of the Pd−Pd NN distance and a concomitant decrease in the Debye−Waller factor; the other coordination numbers and interatomic distances are essentially unchanged. These changes in Pd structure are similar to those that accompany desorption of interstitial hydrogen from monometallic Pd clusters.[10] A significant contribution from segregated Pd clusters is excluded in this case, however, since the Pd−Pd distance after evacuation is significantly longer than that in bulk Pd and the Debye−Waller factor is lower than typically observed for highly dispersed supported Pd.[10] Thus, we conclude that Pd islands are present on the surfaces of Au-rich alloy particles. The Pd−Pd and Pd−Au distances are equivalent after evacuation, and they are in excellent agreement with those observed by Lee et al. for colloidal Au particles covered by an ultrathin Pd layer.[19]

The EXAFS results can be approximated using a cluster "decoration" model in which a Au-rich core is covered by a partial monolayer of Pd. The Pd−Au/SiO_2 (1.3:1, pH 7) EXAFS results are compared in Table 4 to the calculated coordination numbers of a hypothetical Pd-decorated Au cluster. The size of the octahedral Au core was chosen to provide a Au−Au coordination number slightly greater than that determined by EXAFS spectroscopy. A complete monolayer of Pd was then added, requiring a Pd/Au ratio of 2.3. There is reasonable agreement between the observed and calculated Au−Pd coordination numbers; however, the model, as expected, overpredicts the Pd−Pd coordination number and underpredicts the Pd−Au coordination number. Lowering the Pd/Au ratio by removing Pd atoms from the surface will bring the model in closer agreement with experiment, as indicated by the arrows in Table 4. Moving Pd atoms from the surface to the bulk (for a fixed Pd/Au ratio) will reduce the Pd−Pd coordination number and increase the Pd−Au coordination number, further improving the agreement with experiment.

The Pd K and Au L_3 EXAFS results following reduction at 350 °C of Pd−Au/SiO_2 (1:1, pH 10) are indicative of homogeneous Pd−Au alloy clusters. Moreover, the average composition of the alloy clusters is equivalent to the overall composition of the bimetallic catalyst. These conclusions are in agreement with the earlier findings of Lam and Boudart.[8] The total first-shell coordination numbers of the Pd and Au atoms are nearly equal, indicating the absence of surface enrichment, and the Pd and Au atoms are coordinated to approximately equal numbers of like and unlike metal atoms. The Pd−Pd and Au−Au bond distances are equal, and they are in excellent agreement with the value predicted by Vegard's law for a 1:1 Pd−Au alloy (2.815 Å). The heteronuclear NN distances are slightly shorter (∼0.02 Å) than the homonuclear ones, which suggests local ordering due to favorable bond energetics (i.e., $\Delta H_{mix} < 0$).[15] There is no statistically significant difference between the Debye−Waller factors of the homonuclear and heteronuclear bonds. Comparison of the Au $L_{2,3}$ XANES difference spectra of the Pd−Au/SiO_2 (1:1, pH 10) catalyst and the Pd−Au alloy films clearly indicates that the great majority of the Au in the catalyst is alloyed with Pd. Moreover, evacuation of the reduced Pd−Au/SiO_2 (1:1, pH 10) catalyst at 300 °C does not affect the structure of the supported clusters, as evidenced by the coordination numbers and bond distances. Lower Debye−Waller factors are observed, indicating a reduction in static disorder.

The structural differences between the Pd−Au/SiO_2 (1.3:1, pH 7) and Pd−Au/SiO_2 (1:1, pH 10) catalysts are likely the result of kinetic rather than thermodynamic factors. First, the structures of the adsorbed Pd and Au precursor complexes and their initial distributions on silica gel will be influenced by the pH of the exchange solution. For example, adsorption of Pd^{2+} amino complexes on silica at high pH (>10) from aqueous NH_3 solution leads predominantly to electrostatically bound $[Pd(NH_3)_4]^{2+}$, whereas adsorption at lower pH also involves ligand exchange with surface OH groups.[20] These structural differences could alter the reducibility of the Pd precursor. In addition, our observation that $[Au(en)_2]Cl_3$ does not adsorb on silica gel in the absence of $[Pd(NH_3)_4]^{2+}$ indicates that the chemistry is more complicated that simple coadsorption and suggests formation of a Pd−Au bimetallic complex. Second, the observed Pd surface enrichment in the Pd−Au/SiO_2 (1.3:1, pH 7) catalyst may originate from sequential, rather than simultaneous, reduction of Au and Pd ions. The Au L_3 XANES spectrum of this catalyst after impregnation and subsequent drying in air at 100 °C (Figure 6d) is indicative of a mixture of Au^0 and $Au^{\delta+}$ species. The XANES spectrum and the purplish color of the catalyst powder indicate that Au clusters are already present at this stage. The literature indicates that drying of silica gel impregnated with $HAuCl_4$ at 110−130 °C yields supported Au particles (for concentrations not exceeding ∼1 wt % Au).[21] We suggest that (i) Pd atoms generated during reduction at 150 °C migrate to existing Au clusters where they accrete forming

bimetallic particles and (ii) restricted atomic mobility limits the extent of Pd/Au intermixing at this temperature. Lee et al. investigated Pd/Au intermixing in bimetallic colloid particles consisting of 50 Å Au cores coated by a bilayer of Pd atoms.[19] Intermixing was negligible at temperatures less than or equal to 125 °C, and annealing temperatures less than or equal to 300 °C were required for complete intermixing. Since the homogeneously alloyed and Pd surface-enriched samples were pretreated under otherwise equivalent conditions, the higher in situ reduction temperature of the Pd−Au/SiO_2 (1:1, pH 10) catalyst may have resulted in more complete intermixing.

The Au $L_{2,3}$ XANES spectra provide specific information on (i) the unoccupied 5d density of states (DOS) near the Fermi level and (ii) the structure and composition of the Au coordination environment. Consequently, XANES can be used to probe the effects of cluster size and composition on the electronic and structural properties of Pd−Au alloys.[9,22,23] The unoccupied 5d DOS is reflected in the intensities of the 2p → 5d edge resonances (white lines) that appear at approximately 3 eV relative to the edge inflection point. As a consequence of the dipole selection rules, the L_3 white line ($2p_{3/2}$ initial state) probes the total ($d_{3/2} + d_{5/2}$) unoccupied d DOS, and the L_2 white line ($2p_{1/2}$ initial state) probes only the unoccupied $d_{3/2}$ states.[14,24] The atomic state of Au is $d^{10}s^1$; however, s−d and p−d hybridization leads to a finite density of unoccupied d states in bulk Au. A large majority of the unoccupied Au 5d states are expected to have $d_{5/2}$ character due to spin−orbit splitting. Consistent with this hypothesis, a very weak L_3 white line is observed for Au foil, but the L_2 white line has negligible intensity (Figure 7). The similar L_3 white line intensities of the silica-supported Au clusters and Au foil indicate that size effects on electronic structure are minimal for 25−35 Å clusters.[25] Information on the structure and composition of the Au coordination environment can be inferred from XANES features in the 10−50 eV energy range. The XANES features in this range can be interpreted as "multiple scattering resonances" involving a sufficiently large cluster of neighboring atoms.[26] Early multiple scattering (MS) calculations for Cu clusters demonstrated that contributions from pathways involving the first three fcc shells were required to reproduce the experimental K XANES spectrum of bulk Cu.[27] The close similarity between the L_3 XANES spectra of the silica-supported Au clusters and Au foil (Figure 6) indicates that the silica-supported Au clusters have three-dimensional fcc structures.

The Au L_3 XANES difference spectra of the Pd−Au alloy films (Figure 9) each exhibit a similar negative feature near 3 eV resulting from loss of white line intensity. This feature is relatively insensitive to alloy composition, in agreement with a previous report,[23] and indicates a decrease in the density of unoccupied $d_{5/2}$ states relative to bulk Au. A similar loss of L_3 white line intensity is observed for the Pd−Au/SiO_2 catalysts, consistent with the results of Davis et al.[9] We infer that this decrease results from a change in d band hybridization and not from charge transfer, as the extent of charge transfer is small for Pd−Au alloys[28] The rigid band model held that Au donated its 6s electron to the Pd 4d band;[29] however, recent electronic structure calculations[30] and valence band photoemission experiments[31,32] indicate that Pd−Au alloys exhibit split-band rather than mixed-band behavior. As the Pd content is increased, the width and spin−orbit splitting of the Au 5d band decrease, indicating the dominance of like neighbor interactions. XANES spectroscopy of Pd−Au alloys confirms that electron transfer to the Pd 4d band is much smaller than predicted by the rigid band model.[22] Nonetheless, the Pd−Au d−d interaction is believed to have an important effect on the electronic structure of the alloys. In particular, the Au $d^{5/2}$ partial DOS is broadened and shifted to higher binding energy (relative to the Fermi level) with increasing Pd content.[30] The insensitivity of the Au L_3 edge resonance to alloy composition suggests that addition of 20% Pd is sufficient to virtually eliminate unoccupied Au $5d_{5/2}$ states near the Fermi level.

The XANES difference spectra in the 10−50 eV region may be interpreted in terms of MS pathways involving atoms in the first several coordination shells around the Au absorber. We suggest that the composition-dependent peak that appears at 15 eV in the L_2 and L_3 difference spectra arises from MS pathways involving both Pd and Au atoms. Previous workers have used the intensity of this Au L_3 XANES peak to determine the composition of the alloy phase in supported Pd−Au catalysts.[23] A negative peak at 28 eV is also characteristic of Pd−Au alloy formation; it may result from elimination of MS pathways involving only Au atoms. The intensity of this peak is composition dependent at the L_2 edge but insensitive to alloy composition at the L_3 edge. The difference spectra of the Pd−Au/SiO_2 (1:1, pH 10) catalyst are consistent with a 50% Au alloy, in agreement with the overall catalyst composition and the composition of the Au first coordination shell as determined by EXAFS spectroscopy. The difference spectra of the Pd−Au/SiO_2 (1.3:1, pH 7) catalyst are in good agreement with those of the 60% Au alloy film, as would be expected from the Au L_3 EXAFS results.

Conclusions

The Pd−Au/SiO_2 (1.3:1, pH 7) catalyst that was reduced at 300 °C contains bimetallic clusters consisting of a Au-rich core decorated by Pd. In contrast, the Pd−Au/SiO_2 (1:1, pH 10) catalyst that was reduced at 350 °C contains homogeneous Pd−Au alloy clusters. The observed Pd surface enrichment in the Pd−Au/SiO_2 (1.3:1, pH 7) catalyst may originate from sequential, rather than simultaneous, reduction of Au and Pd ions during catalyst preparation. The Au L_3 XANES difference spectra of the supported Pd−Au clusters and a series of Pd−Au alloy films exhibit a similar negative feature near 3 eV resulting from loss of white line intensity. This feature is relatively insensitive to alloy composition and indicates a decrease in the density of unoccupied Au 5d states relative to bulk Au. MS features in the 10−50 eV region of the Au $L_{2,3}$ XANES spectra are also affected by Pd−Au alloying. The intensity of the positive peak at 15 eV in the L_2 and L_3 difference spectra increases proportionately with Pd concentration.

Acknowledgment. The Pd−Au films were provided by Dr. James A. McCaulley of the Hoechst-Celanese Corporation. This work was partially supported by an NSF Presidential Young Investigator Award (CTS-8958350). S.N.R. gratefully acknowledges a Ph.D. fellowship from Hoechst-Celanese Corporation. The authors thank Prof. D. E. Sayers and the staff of beamline X-11 at the National Synchrotron Light Source for their assistance.

References and Notes

(1) Nakamura, M.; Fujiwara, Y.; Yasui, T. U.S. Patent 4,087,622, 1978.
(2) Sennewald, K.; Glaser, H. U.S. Patent 3,761,513, 1973.
(3) Somorjai, G. A. *Introduction to Surface Chemistry and Catalysis*; John Wiley & Sons: New York, 1994.
(4) Rainer, D. R.; Xu, C.; Holmblad, P. M.; Goodman, D. W. *J. Vac. Sci. Technol. A* **1997**, *15*, 1653.
(5) Baddeley, C. J.; Tikhov, M.; Hardacre, C.; Lomas, J. R.; Lambert, R. M. *J. Phys. Chem.* **1996**, *100*, 2189.
(6) Sinfelt, J. H. *Bimetallic Catalysts: Discoveries, Concepts, and Applications*; John Wiley & Sons: New York, 1983.

(7) Via, G. H.; Drake, K. F., Jr.; Meitzner, G.; Lytle, F. W.; Sinfelt, J. H. *Catal. Lett.* **1990**, *5*, 25.
(8) Lam, Y. L.; Boudart, M. *J. Catal.* **1977**, *50*, 530.
(9) Davis, R. J.; Boudart, M. *J. Phys. Chem.* **1994**, *98*, 5471.
(10) Reifsnyder, S. N.; Lamb, H. H. *Catal. Lett.* **1996**, *40*, 155.
(11) Sayers, D. E.; Bunker, B. A. In *X-ray Absorption: Principles, Applications, Techniques of EXAFS, SEXAFS, and XANES*; Koningsberger, D. C., Prins, R., Eds.; John Wiley & Sons: New York, 1988; p 211.
(12) Vaarkamp, M.; Linders, J. C.; Koningsberger, D. C. *Physica B* **1995**, *208*/*209*, 159.
(13) Mustre de Leon, J.; Rehr, J. J.; Zabinsky, S. I.; Albers, R. C. *Phys. Rev. B* **1991**, *44*, 4146.
(14) Mansour, A. N.; Cook, J. W., Jr.; Sayers, D. E. *J. Phys. Chem.* **1984**, *88*, 2330.
(15) Darby, J. B., Jr. *Acta Metall.* **1966**, *14*, 265.
(16) Maire, G.; Hilaire, L.; Legare, P.; Gault, F. G.; O'Cinneide, A. *J. Catal.* **1976**, *44*, 293.
(17) Wood, B. J.; Wise, H. *Surf. Sci.* **1975**, *52*, 151.
(18) Vázquez, A.; Pedraza, F.; Gómez, A. *Appl. Surf. Sci.* **1992**, *55*, 221.
(19) Lee, A. F.; Baddeley, C. J.; Hardacre, C.; Ormerod, R. M.; Lambert, R. M. *J. Phys. Chem.* **1995**, *99*, 6096.
(20) Spielbauer, D.; Zeilinger, H.; Knözinger, H. *Langmuir* **1993**, *9*, 460.
(21) Bond, G. C.; Sermon, P. A. *J. Chem. Soc., Chem. Commun.* **1973**, 444.
(22) Meitzner, G.; Sinfelt, J. H. *Catal. Lett.* **1995**, *30*, 1.
(23) Couves, J. W.; Meehan, P. *Physica B* **1995**, *208/209*, 665.
(24) Brown, M.; Peierls, R. E.; Stern, E. A. *Phys. Rev. B* **1977**, *15*, 738.
(25) Balerna, A.; Bernieri, E.; Picozzi, P.; Reale, A.; Santucci, S.; Burattini, E.; Mobilio, S. *Phys. Rev. B* **1985**, *31*, 5058.
(26) Bianconi, A. In *X-ray Absorption: Principles, Applications, Techniques of EXAFS, SEXAFS, and XANES*; Koningsberger, D. C., Prins, R., Eds.; John Wiley & Sons: New York, 1988; p 573.
(27) Greaves, G. N.; Durham, P. J.; Diakun, G.; Quinn, P. *Nature* **1981**, *294*, 4960.
(28) Nascente, P. A. P.; Castro, S. G. C. d.; Landers, R.; Kleiman, G. G. *Phys. Rev. B* **1991**, *43*, 4659.
(29) Mott, N.; Jones, H. *Theory of Metals and Alloys*; Clarendon Press: Oxford, 1936.
(30) Weinberger, P.; Szunyogh, L.; Bennett, B. I. *Phys. Rev. B* **1993**, *47*, 10154.
(31) Blyth, R. I. R.; Andrews, A. B.; Arko, A. J.; Joyce, J. J.; Canfield, P. C.; Bennett, B. I. *Phys. Rev. B* **1994**, *49*, 16149.
(32) Nicholson, J. A.; Riley, J. D.; Leckey, R. C. G.; Jenkin, J. G.; Liesegang, J. *J. Electron Spectrosc. Relat. Phenom.* **1979**, *15*, 95.